Journal of Biomolecular NMR (2005) 32: 113–127
DOI 10.1007/s10858-005-5618-z

Article

qTROSY – a novel scheme for recovery of the anti-TROSY magnetisation

Tammo Diercks[a,b] & Vladislav Y. Orekhov[a,*]
[a]*Swedish NMR Centre at Göteborg University, P.O.Box 465Göteborg, SE 40530, Sweden;* [b]*Department of NMR Spectroscopy, Bijvoet Center for Biomolecular Research, Utrecht University, 3584, CH, Utrecht, The Netherlands*

Received 15 December 2004; Accepted 7 April 2005

Key words: cross-correlated relaxation, magnetisation recovery, orthogonal spin state separation, queued spectroscopy, TROSY

Abstract

In TROSY experiments, spin state selection (S^3) retains only the single HSQC sub-spectrum with minimal T_2 relaxation and maximal resolution, yet at the cost of eliminating half of the available polarisation as undesired anti-TROSY component. We here introduce queued TROSY (qTROSY) as a novel scheme to partially recover and exploit this anti-TROSY polarisation in two concatenated scans. After initial orthogonal spin state separation (oS^3), anti-TROSY polarisation is explicitly stored while its TROSY counterpart follows the desired coherence pathway recorded in a first scan A. The immediately appended scan B then quantitatively converts the recovered anti-TROSY polarisation into a second TROSY spectrum, skipping the time-limiting long reequilibration delay. Both concatenated qTROSY scans thus ideally exploit the full initial polarisation within almost the same measurement time. In practice, T_2 relaxation losses accruing during the coupling evolution delays reduced anti-TROSY polarisation recovery below 40%, obviating sensitivity enhancement through addition of both qTROSY scans; yet, scan B retained a complete scan A spectrum with up to 75% intensity. We therefore propose to employ qTROSY asymmetrically, compacting two separate conventional into one queued TROSY-type experiment with significantly reduced measurement time, implying primarily the concatenation of different three- or higher-dimensional experiments. Both anti-TROSY polarisation recoveries and possible time savings are largest for deuterated and smaller non-deuterated proteins, extending the rentability limit of the TROSY principle towards smaller molecular weights.

Abbreviations: oS^3 – orthogonal spin state separation; S^3 – spin state selective; S^3-CT – S^3 coherence transfer; S^3E – S^3 excitation; ST2-PT – spin state to spin state selective polarisation transfer.

Introduction

NMR spectroscopy is by now established as a most versatile technique to address the challenging problems of structural biology, including molecular dynamics and binding studies. The TROSY principle (Pervushin et al., 1997) thereby has substantially extended the molecular size limit of NMR, recording only the one spin state selective (S^3) sub-spectrum with a maximal cancellation of detrimental relaxation processes. This results primarily in considerably sharpened signals, and thus improved spectral resolution for biomolecules. Spin state selection, however, inevitably comes at the cost of splitting the total polarisation equally

*To whom correspondence should be addressed. E-mail: orov@nmr.se

into two (for 1/2-spins), only half of which is converted into the desired TROSY signal. The complementary anti-TROSY component has so far mostly been discarded through phase cycling (Pervushin et al., 1998) or pulsed field gradients (Palmer et al., 1991; Czisch and Boelens, 1998; Weigelt, 1998), except in a few schemes to retain anti-TROSY along with the TROSY coherence after its modulation by chemical shift and transverse relaxation (Andersson et al., 1998; Schulte-Herbrüggen et al., 1999). Although to some extent compensated by reduced relaxation losses especially for larger biomolecules, the initial sacrifice of half the available polarisation thus remains a dissatisfactory aspect of TROSY spectroscopy.

We here present queued TROSY (qTROSY) as a novel and broadly applicable scheme to restore anti-TROSY polarisation, rather than coherence, and independently exploit it after conversion into genuine TROSY magnetisation. The decisive feature of qTROSY is orthogonal spin state separation, oS^3, in the initial preparatory module prior to any chemical shift evolution with concomitant T_2 relaxation decay. Contrary to conventional TROSY implementations, this explicitly generates both complementary heteronuclear S^3 components as separable orthogonal magnetisations – transverse TROSY coherence and longitudinal anti-TROSY polarisation (strictly speaking, the term TROSY, Transverse Relaxation Optimised Spectroscopy, cannot be used with polarisations; we still prefer to use it for easy recognition of the same coupled spin state). Of these, only the TROSY coherence is modulated during a subsequent indirect evolution time by chemical shift and T_2 relaxation. Both components are then transferred spin state selectively from the heteronucleus to its attached proton, allowing conventional acquisition of the TROSY spectrum on the coherence part while the ^{1}H anti-TROSY polarisation again passes FID acquisition without modulation. It can now be exploited as well, after S^3 conversion into TROSY coherence, in an immediately appended (queued) second scan.

Our qTROSY scheme thus ideally converts all initial polarisation into TROSY coherence in two concatenated scans without the inter-scan reequilibration delay that usually dominates experiment durations. Within almost the same time, qTROSY could thus exploit up to twice as much magnetisation as conventional TROSY implementations. In practice, recovery of the 50% anti-TROSY polarisation is limited primarily by relaxation losses, directing how the additional magnetisation sampled by the queued second scan should be exploited: (i) It could either be used in a repetition of the *same* experiment, yielding identical spectra for both scans that can then be added up (with a concomitant increase in noise by $\sqrt{2}$) for sensitivity enhancement provided the second scan recovers more than $\sqrt{2}-1 \approx 40\%$ of the first scan's intensities. (ii) Alternatively, the second scan could record a *different* experiment, precluding spectrum and, hence, noise addition. No strict rentability threshold applies in such *asymmetric qTROSY* experiments that compact two into one TROSY-type experiment within almost the same measurement time; the less sensitive second scan must only retain sufficient intensity for a complete spectrum also.

With these two possible ways of exploiting the recovered anti-TROSY magnetisation, qTROSY should especially extend the attractiveness of TROSY-type experiments to deuterated and smaller proteins that, owing to favourable relaxation properties, offer particularly high anti-TROSY recovery rates. Thus, even the smaller proteins (ca. 100 residues) that still form the bulk of NMR-relevant biomolecules could benefit from the general line-sharpening from TROSY selection without inacceptable costs in sensitivity. Simultaneously recording two spectra while skipping every other long reequilibration delay should, on the other hand, prove particularly attractive for deuterated proteins with their substantially prolonged T_1 relaxation times, representing the favourite substrates for TROSY-type experiments.

Description of the qTROSY scheme

The pulse sequence for the basic double-scan qTROSY experiment is depicted in Figure 1 and described modularly in the following, with a detailed analysis of all relevant magnetisation paths employing standard operator formalism (Soerensen et al., 1983). Both concatenated scans of qTROSY differ only in their preparatory parts and will henceforth be referred to as scans A and B. All other modules – indirect T_1 evolution time, S^3 magnetisation back-transfer from ^{15}N to ^{1}H, coherence selection and FID acquisition – are identical and correspond to known technique. All

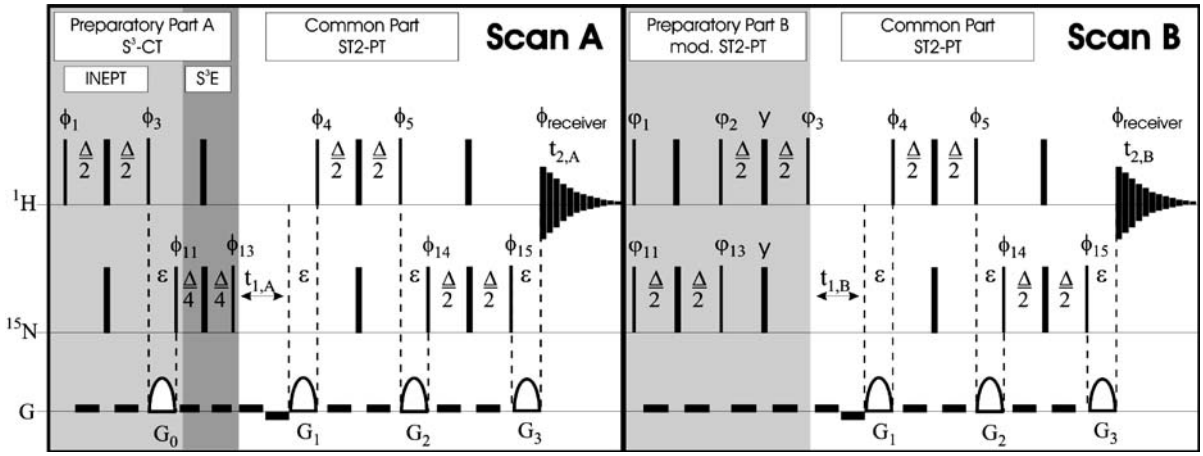

Figure 1. qTROSY pulse sequence. In the concatenated double-scan scheme, only the preparatory parts differ for scans A and B. $\Delta \leq 1/2^1J_{HN}$. Pulse phases as required on VARIAN Inova (x = default): $\phi_1 = y$; $\phi_3 = x$; $\phi_{11} = 45°$, 45°, 225°, 225°; $\phi_{13} = y, y, -y, -y$; $\varphi_1 = y$; $\varphi_2 = y$; $\varphi_3 = x$; $\varphi_{11} = y, y, -y, -y$; $\varphi_{13} = x, x, -x, -x$; $\phi_4 = x$; $\phi_5 = y$; $\phi_{14} = x, -x$; $\phi_{15} = y, -y$; $\phi_{rec.} = x, -x, -x, x$. For antiecho detection in t_1 with preservation of flip-back for water and the stored ^{1}H anti-TROSY polarisation at the end of scan A, phases ϕ_5, ϕ_{15}, ϕ_1, ϕ_3 and ϕ_{13} must be inverted. Axial peaks are shifted to the spectral edges by inverting phases ϕ_{11}, ϕ_{13}, φ_{11}, φ_{13} and the receiver for successive time increments. Open gradients $G_{1\text{-}3}$ of equal duration ε select for ^{15}N coherence in t_1, intermediate ^{15}N, ^{1}H zero- (echo) or double-quantum coherence (antiecho), and ^{1}H coherence during acquisition by setting $G_1 = -3.44a$, $G_2 = 1.5a$, $G_3 = 2a$ (echo) and $G_3 = a$ (antiecho) with a = arbitrary gradient amplitude; $G_0 = G_1$ for preservation of water flip-back. The weak filled gradient pairs are used to suppress radiation damping (Sklenar, 1995). For the given phases, natural ^{15}N polarization is added to the TROSY magnetisation sampled in scan A, but can be shuffled to the anti-TROSY magnetisation sampled in scan B by inverting phases ϕ_3, ϕ_{13} and φ_1. Optionally, natural ^{15}N polarization can be obliterated by preceding scan A with a 90° pulse on ^{15}N, followed by a strong z-spoil gradient. Scan A can be modified to simulate a conventional TROSY by simply omitting the S^{3}E module and inverting G_0, maintaining ^{15}N polarisation enhancement and water flip-back.

calculations derive from one basic commutator rule:

$$\lfloor I_j, I_{j+1} \rfloor = \mathrm{sign}(\gamma_I) \cdot iI_{j+2}, \tag{1}$$

where $j = x, y, z$ and cyclic permutations thereof. These commutators define a right-handed cartesian coordinate system for ^{1}H (with positive γ_H) and a left-handed one for ^{15}N (with negative γ_N), whence pulses and couplings effect opposite rotations for both nuclei. Furthermore, remember that $^1J_{HN}$ is negative. These basic initial conventions provide full agreement between theory and experiment on the assumption of identity between theoretical and spectrometer phases (valid for our VARIAN Inova spectrometer; different phase settings may be required on other spectrometers). In fact, consistency only requires spectrometer phases to be equal on both channels used for ^{1}H and ^{15}N.

Preparatory S^3-CT module of scan A

Central to the qTROSY scheme, scan A must initially prepare *orthogonally separated* $N_y(\frac{1}{2} + H_z)$ TROSY *coherence* and $N_z(\frac{1}{2} - H_z)$ anti-TROSY *polarisation* prior to any shift evolution time. This can be achieved using the S^3-CT module (Meissner et al., 1997), where the initial INEPT, preparing hyperpolarised $2H_zN_z$ spin order, is complemented by a S^{3}E module to evolve orthogonally separated ^{15}N TROSY and anti-TROSY coherences during an additional delay $(4^1J_{HN})^{-1}$:

$$-2\gamma_H N_z H_z \xrightarrow{90^\circ_{45^\circ}(^{15}N)} \frac{2}{\sqrt{2}}\gamma_H[N_x H_z - N_y H_z]$$
$$\xrightarrow[180^\circ_x(^1H,^{15}N)]{\pi J[2H_zN_z]\cdot(4J)^{-1}} -\gamma_H N_y\left(\tfrac{1}{2} + H_z\right) + \gamma_H N_x\left(\tfrac{1}{2} - H_z\right) \tag{2a}$$

As in conventional TROSY (Pervushin et al., 1998), natural $\gamma_N \cdot N_z$ polarisation contributes $|\gamma_N/\gamma_H| = 10\%$ additional intensity unless explicitly eliminated, e.g. by alternatingly inverting the INEPT module, or inserting an initial 90°(^{15}N) excitation pulse followed by a dephasing z-spoil gradient:

$$\xrightarrow{180^\circ(^{15}\mathrm{N})} -\gamma_\mathrm{N}\mathrm{N}_z \xrightarrow{90^\circ_{45^\circ}(^{15}\mathrm{N})} \frac{\gamma_\mathrm{N}}{\sqrt{2}}\left[\mathrm{N}_x - \mathrm{N}_y\right]$$
$$\xrightarrow[180^\circ_x(^1\mathrm{H},^{15}\mathrm{N})]{\pi J[2\mathrm{H}_z\mathrm{N}_z]\cdot(4J)^{-1}} \gamma_\mathrm{N}\mathrm{N}_y\left(\tfrac{1}{2}+\mathrm{H}_z\right) + \gamma_\mathrm{N}\mathrm{N}_x\left(\tfrac{1}{2}-\mathrm{H}_z\right) \tag{2b}$$

A final 90°(^{15}N) flip-back pulse along y then restores the anti-TROSY N_x $(\frac{1}{2} - \mathrm{H}_z)$ coherence as $\mathrm{N}_z(\frac{1}{2} - \mathrm{H}_z)$ polarisation. In combination, INEPT (2a) and γ_N-derived (2b) paths produce:

$$-\{\gamma_\mathrm{H}-\gamma_\mathrm{N}\}\mathrm{N}_y\left(\tfrac{1}{2}+\mathrm{H}_z\right)+\{\gamma_\mathrm{H}+\gamma_\mathrm{N}\}\mathrm{N}_x\left(\tfrac{1}{2}-\mathrm{H}_z\right)$$
$$\xrightarrow{90^\circ_y(^{15}\mathrm{N})} -\{\gamma_\mathrm{H}-\gamma_\mathrm{N}\}\mathrm{N}_y\left(\tfrac{1}{2}+\mathrm{H}_z\right)+\{\gamma_\mathrm{H}+\gamma_\mathrm{N}\}\mathrm{N}_z\left(\tfrac{1}{2}-\mathrm{H}_z\right) \tag{3}$$

subsequent indirect chemical shift evolution period $t_{1,\mathrm{A}}$. The terminal ST2-PT module (Pervushin et al., 1998) then transfers both S^3 coherence and polarisation from ^{15}N to H^N with preservation of spin states. Pulse imperfections, incomplete spin-state separation by the initial S^3-CT module, and cross-talk relaxation (Meissner et al., 1998b), however, invariably cause some mixture of proton spin states for the desired $\mathrm{N}_y(\frac{1}{2} + \mathrm{H}_z)$ coherence and $\mathrm{N}_y(\frac{1}{2} - \mathrm{H}_z)$ polarisation. Equation 4 summarises the conversion of desired (top 3 rows) and unwanted magnetisations (bottom 3 rows; here and in the following separated by horizontal lines).

$$\underbrace{\begin{pmatrix}\mathrm{N}_x(\frac{1}{2}+\mathrm{H}_z)\\ \mathrm{N}_y(\frac{1}{2}+\mathrm{H}_z)\\ \mathrm{N}_z(\frac{1}{2}-\mathrm{H}_z)\\ \hline \mathrm{N}_x(\frac{1}{2}-\mathrm{H}_z)\\ \mathrm{N}_y(\frac{1}{2}-\mathrm{H}_z)\\ \mathrm{N}_z(\frac{1}{2}+\mathrm{H}_z)\end{pmatrix}}_{\text{at } G_1} \xrightarrow[3)\,\pi J[2\mathrm{H}_z\mathrm{N}_z]\cdot(2J)^{-1}]{\substack{1)\ 90^\circ_x(^1\mathrm{H})\\ 2)\ 180^\circ_x(^1\mathrm{H}^{15}\mathrm{N})}} \begin{pmatrix}\mathrm{N}_y\mathrm{H}_z+\mathrm{N}_x\mathrm{H}_y\\ \mathrm{N}_x\mathrm{H}_z-\mathrm{N}_y\mathrm{H}_y\\ -\frac{1}{2}\mathrm{N}_z+\frac{1}{2}\mathrm{H}_x\\ \hline \mathrm{N}_y\mathrm{H}_z-\mathrm{N}_x\mathrm{H}_y\\ \mathrm{N}_x\mathrm{H}_z+\mathrm{N}_y\mathrm{H}_y\\ -\frac{1}{2}\mathrm{N}_z-\frac{1}{2}\mathrm{H}_x\end{pmatrix} \xrightarrow{\pm 90^\circ_y(^1\mathrm{H})} \underbrace{\begin{pmatrix}\pm\mathrm{N}_y\mathrm{H}_x+\mathrm{N}_x\mathrm{H}_y\\ \pm\mathrm{N}_x\mathrm{H}_x-\mathrm{N}_y\mathrm{H}_y\\ -\frac{1}{2}\mathrm{N}_z\mp\frac{1}{2}\mathrm{H}_z\\ \hline \pm\mathrm{N}_y\mathrm{H}_x-\mathrm{N}_x\mathrm{H}_y\\ \pm\mathrm{N}_x\mathrm{H}_x+\mathrm{N}_y\mathrm{H}_y\\ -\frac{1}{2}\mathrm{N}_z\pm\frac{1}{2}\mathrm{H}_z\end{pmatrix}}_{\text{at } G_2} \xrightarrow[3)\,\pi J[2\mathrm{H}_z\mathrm{N}_z]\cdot(2J)^{-1}]{\substack{1)\ 90^\circ_x(^{15}\mathrm{N})\\ 2)\ 180^\circ_x(^1\mathrm{H}^{15}\mathrm{N})}} \begin{pmatrix}\mp\frac{1}{2}\mathrm{H}_y-\mathrm{N}_x\mathrm{H}_y\\ \pm\mathrm{N}_x\mathrm{H}_x+\frac{1}{2}\mathrm{H}_x\\ -\mathrm{N}_x\mathrm{H}_z\pm\frac{1}{2}\mathrm{H}_z\\ \hline \mp\frac{1}{2}\mathrm{H}_y+\mathrm{N}_x\mathrm{H}_y\\ \pm\mathrm{N}_x\mathrm{H}_x-\frac{1}{2}\mathrm{H}_x\\ -\mathrm{N}_x\mathrm{H}_z\mp\frac{1}{2}\mathrm{H}_z\end{pmatrix} \xrightarrow{\pm 90^\circ_y(^{15}\mathrm{N})} \underbrace{\begin{pmatrix}\mp\mathrm{H}_y(\frac{1}{2}+\mathrm{N}_z)\\ \mathrm{H}_x(\frac{1}{2}+\mathrm{N}_z)\\ \pm\mathrm{H}_z(\frac{1}{2}-\mathrm{N}_z)\\ \hline \mathrm{H}_y(\frac{1}{2}-\mathrm{N}_z)\\ -\mathrm{H}_x(\frac{1}{2}-\mathrm{N}_z)\\ \mp\mathrm{H}_z(\frac{1}{2}+\mathrm{N}_z)\end{pmatrix}}_{\text{at } G_3} \tag{4}$$

H^N and ^{15}N polarisations thus add up on only one S^3 component at the expense of its S^3 counterpart, where the chosen phase setting adds the ^{15}N polarisation enhancement to the TROSY coherence observed in scan A (cf. negative γ_N). This can be swapped to scan B enhancement by inverting the INEPT part (phase ϕ_3) along with ϕ_{13} to avoid inversion of the stored anti-TROSY polarisation. For clarity, enhancement factors $\{\gamma_\mathrm{H} \pm \gamma_\mathrm{N}\}$ will be omitted from now on.

Terminal ST2-PT module of scan A

As required, the stored $\mathrm{N}_z(\frac{1}{2} - \mathrm{H}_z)$ anti-TROSY polarisation remains unmodulated during the

The ST2-PT module thus simultaneously transfers $\mathrm{N}_{xy}(\frac{1}{2} + \mathrm{H}_z)$ to $\mathrm{H}_{yx}(\frac{1}{2} + \mathrm{N}_z)$ TROSY coherence (rows 1 and 2) and $\mathrm{N}_z(\frac{1}{2} - \mathrm{H}_z)$ to $\mathrm{H}_z(\frac{1}{2} - \mathrm{N}_z)$ anti-TROSY polarisation (row 3). Yet, the unwanted side components – anti-TROSY coherence (rows 4 and 5) and TROSY polarisation (row 6) – are likewise preserved and transferred from ^{15}N to H^N. Equation 4 also considers inversion of the final 90°_y pulse (phases ϕ_5 and ϕ_{15}) in each half of the ST2-PT module, as required for hyper-complex data acquisition in F1 (Czisch and Boelens, 1998) to project either N^+ (echo) or N^- (antiecho) onto the observed H^- coherence. The corresponding transformation from Cartesian to rotating frame is achieved by computing complex sums and differences of orthogonal N_x and N_y S^3 coherences (rows $1 \pm 2{\cdot}i$ and $4 \pm 5{\cdot}i$, respectively Equation 5a):

$$\begin{pmatrix}\mathbf{1+2\cdot i}\\ \mathbf{1-2\cdot i}\\ \mathbf{3}\\ \hline \mathbf{4+5\cdot i}\\ \mathbf{4-5\cdot i}\\ \mathbf{6}\end{pmatrix} \Rightarrow -\underbrace{\begin{pmatrix}[\mathrm{N}_x+i\mathrm{N}_y](\frac{1}{2}+\mathrm{H}_z)\\ [\mathrm{N}_x-i\mathrm{N}_y](\frac{1}{2}+\mathrm{H}_z)\\ \mathrm{N}_z(\frac{1}{2}-\mathrm{H}_z)\\ \hline [\mathrm{N}_x+i\mathrm{N}_y](\frac{1}{2}-\mathrm{H}_z)\\ [\mathrm{N}_x-i\mathrm{N}_y](\frac{1}{2}-\mathrm{H}_z)\\ \mathrm{N}_z(\frac{1}{2}+\mathrm{H}_z)\end{pmatrix}}_{\text{at } G_1} \xrightarrow[1.\text{half}]{\text{ST2-PT}(\pm)} \underbrace{\begin{pmatrix}[\pm\mathrm{N}_y\mathrm{H}_x+\mathrm{N}_x\mathrm{H}_y]+i[\pm\mathrm{N}_x\mathrm{H}_x-\mathrm{N}_y\mathrm{H}_y]\equiv[\mathrm{N}_x-i\mathrm{N}_y]\cdot[\mathrm{H}_x\mp i\mathrm{H}_y]\\ [\pm\mathrm{N}_y\mathrm{H}_x+\mathrm{N}_x\mathrm{H}_y]-i[\pm\mathrm{N}_x\mathrm{H}_x-\mathrm{N}_y\mathrm{H}_y]\equiv[\mathrm{N}_x+i\mathrm{N}_y]\cdot[\mathrm{H}_x\pm i\mathrm{H}_y]\\ -\frac{1}{2}[\mathrm{N}_z\pm\mathrm{H}_z]\\ \hline [\pm\mathrm{N}_y\mathrm{H}_x-\mathrm{N}_x\mathrm{H}_y]+i[\pm\mathrm{N}_x\mathrm{H}_x+\mathrm{N}_y\mathrm{H}_y]\equiv[\mathrm{N}_x-i\mathrm{N}_y]\cdot[\mathrm{H}_x\pm i\mathrm{H}_y]\\ [\pm\mathrm{N}_y\mathrm{H}_x-\mathrm{N}_x\mathrm{H}_y]-i[\pm\mathrm{N}_x\mathrm{H}_x+\mathrm{N}_y\mathrm{H}_y]\equiv[\mathrm{N}_x+i\mathrm{N}_y]\cdot[\mathrm{H}_x\mp i\mathrm{H}_y]\\ -\frac{1}{2}[\mathrm{N}_z\mp\mathrm{H}_z]\end{pmatrix}}_{\text{at } G_2} \xrightarrow[2.\text{half}]{\text{ST2-PT}(\pm)} \underbrace{\begin{pmatrix}[\mathrm{H}_x\pm i\mathrm{H}_y](\frac{1}{2}+\mathrm{N}_z)\\ [\mathrm{H}_x\mp i\mathrm{H}_y](\frac{1}{2}+\mathrm{N}_z)\\ \pm\mathrm{H}_z(\frac{1}{2}-\mathrm{N}_z)\\ \hline [\mathrm{H}_x\mp i\mathrm{H}_y](\frac{1}{2}-\mathrm{N}_z)\\ [\mathrm{H}_x\pm i\mathrm{H}_y](\frac{1}{2}-\mathrm{N}_z)\\ \mp\mathrm{H}_z(\frac{1}{2}+\mathrm{N}_z)\end{pmatrix}}_{\text{at } G_3} \tag{5a}$$

Substitution by shift operators $I^{\pm} = I_x \pm \mathrm{sign}(\gamma_I) \cdot iI_y$, $ZQ^{\pm} = I^{\pm}S^{\mp}$, $DQ^{\pm} = I^{\pm}S^{\pm}$ and $DQ_z/ZQ_z = \frac{1}{2}[I_z \pm S_z]$ simplifies the ST2-PT transfer matrix to Equation 5b:

$$\underbrace{\begin{pmatrix} N^-(\frac{1}{2}+H_z) \\ N^+(\frac{1}{2}+H_z) \\ N_z(\frac{1}{2}-H_z) \\ \hline N^-(\frac{1}{2}-H_z) \\ N^+(\frac{1}{2}-H_z) \\ N_z(\frac{1}{2}+H_z) \end{pmatrix}}_{\text{at } G_1} \xrightarrow[\text{1.half}]{\text{ST2-PT}(+|-)} \underbrace{\begin{pmatrix} N^+H^- & | & N^+H^+ \\ N^-H^+ & | & N^-H^- \\ -\frac{1}{2}[H_z+N_z] & | & \underline{-\frac{1}{2}[H_z-N_z]} \\ \hline N^+N^+ & | & zN^+N^- \\ N^-H^- & | & N^-H^+ \\ \frac{1}{2}[H_z-N_z] & | & -\frac{1}{2}[H_z+N_z] \end{pmatrix}}_{\text{at } G_2} \equiv \begin{pmatrix} ZQ^- & | & DQ^+ \\ ZQ^+ & | & DQ^- \\ \underline{-DQ_z} & | & \underline{ZQ_z} \\ DQ^+ & | & ZQ^- \\ DQ^- & | & ZQ^+ \\ ZQ_z & | & -DQ_z \end{pmatrix} \xrightarrow[\text{2.half}]{\text{ST2-PT}(+|-)} \underbrace{\begin{pmatrix} H^+(\frac{1}{2}+N_z) & | & H^-(\frac{1}{2}+N_z) \\ H^-(\frac{1}{2}+N_z) & | & H^+(\frac{1}{2}+N_z) \\ H_z(\frac{1}{2}-N_z) & | & -H_z(\frac{1}{2}-N_z) \\ \hline H^-(\frac{1}{2}-N_z) & | & H^+(\frac{1}{2}-N_z) \\ H^+(\frac{1}{2}-N_z) & | & H^-(\frac{1}{2}-N_z) \\ -H_z(\frac{1}{2}+N_z) & | & H_z(\frac{1}{2}+N_z) \end{pmatrix}}_{\text{at } G_3} \tag{5b}$$

where ST2-PT(+|−) corresponds to phases ϕ_5 and ϕ_{15} being set to $+y$ or $-y$, respectively, with the associated terms separated by a vertical line. Equation 5b reveals that a previously published scheme for the direct selection of the TROSY coherence path (rows 1 and 2) using *three* z-gradients $G_{1\text{-}3}$ (Meissner et al., 1998a) would not interfere with the anti-TROSY polarisation path (row 3) also required in qTROSY, as the latter remains aligned along z during all gradients. This triple gradient scheme achieves S^3 *coherence selection in a single scan* with the additional gradient G_2 missing in conventional double gradient schemes (Palmer et al., 1991; Czisch and Boelens, 1998; Weigelt, 1998), since only at this center point of the ST2-PT module do TROSY (rows 1 and 2) and anti-TROSY (rows 4 and 5) coherence paths adopt distinctly different multi-quantum coherences (i.e., DQ|ZQ vs. ZQ|DQ). The triple gradient scheme must thus select the following echo and antiecho coherence paths:

echo path = row 2 with ST2-PT(+):

$$\underbrace{N^+\left(\tfrac{1}{2}+H_z\right)}_{\propto\gamma_N\cdot G_1} \xrightarrow[\text{1.half}]{\text{ST2-PT}(+)} \underbrace{N^-H^+ \equiv ZQ^+}_{\propto[\gamma_H-\gamma_N]\cdot G_2} \xrightarrow[\text{2.half}]{\text{ST2-PT}(+)} \underbrace{H^-\left(\tfrac{1}{2}+N_z\right)}_{\propto-\gamma_H\cdot G_3} \tag{6a}$$

antiecho path = row 1 with ST2-PT(−):

$$\underbrace{N^-\left(\tfrac{1}{2}+H_z\right)}_{\propto-\gamma_N\cdot G_1} \xrightarrow[\text{1.half}]{\text{ST2-PT}(-)} \underbrace{N^+H^+ \equiv DQ^+}_{\propto[\gamma_H+\gamma_N]\cdot G_2} \xrightarrow[\text{2.half}]{\text{ST2-PT}(-)} \underbrace{H^-\left(\tfrac{1}{2}+N_z\right)}_{\propto-\gamma_H\cdot G_3} \tag{6b}$$

With $\gamma_H \approx -9.87\gamma_N$, a possible gradient ratio is $G_1 = -3.44\alpha$, $G_2 = 1.5\alpha$, $G_3 = 2\alpha$ for the echo path and $G_3 = \alpha$ for the antiecho path, where $\alpha =$ arbitrary gradient amplitude, and all gradients have *equal* duration ε. In this case, the rephasing property inherent to each half of the ST2-PT module exactly cancels chemical shift evolution during ε for both ^{15}N (first half) and ^{1}H (second half). The triple-gradient selection scheme thus actually shortens the pulse sequence by one gradient duration ε normally inserted for chemical shift refocussing. While none of the three z-gradients has any effect on the transfer path for the stored anti-TROSY polarisation (row 3), suppression of the TROSY polarisation side component (row 6) is impossible for the same reason.

By the end of scan A, the following desired main components with their corresponding weighting factors remain:

$$\xi^A \cdot [\gamma_H \mp \gamma_N] \cdot H^-(\tfrac{1}{2}+N_z) = H^N \text{ TROSY coherence (observed in scan A)} \tag{7a}$$

$$\xi^A \cdot [\gamma_H \pm \gamma_N] \cdot H_z(\tfrac{1}{2}-N_z) = H^N \text{ anti-TROSY polarisation (stored for scan B)} \tag{7b}$$

As described in section "Preparatory S^3-CT module of scan A", the phase setting there determines where natural ^{15}N polarisation is added ($-\gamma_N$) or subtracted ($+\gamma_N$). The scaling factor $\xi^A < 1$ comprises all losses due to relaxation, pulse imperfections, or incomplete spin state separation. A third undesired, yet unobservable side component at the end of scan A is:

$$-(1-\xi^A) \cdot [\gamma_H \pm \gamma_N] \cdot H_z(\tfrac{1}{2}+N_z) = H^N \text{ TROSY polarisation (side component)} \tag{7c}$$

The triple-gradient selection scheme, however, eliminates any unwanted anti-TROSY coherence, $(1-\xi^{A})\cdot[\gamma_{H}\mp\gamma_{N}]\cdot H^{-}(\frac{1}{2}-N_z)$.

$$\begin{pmatrix}\xi^{B}[\gamma_{H}\pm\gamma_{N}]\\ \hline (1-\xi^{B})[\gamma_{H}\mp\gamma_{N}]\\ \zeta\gamma_{N}\end{pmatrix}\cdot\left\{\begin{pmatrix}H_z(\frac{1}{2}-N_z)\\ \hline -H_z(\frac{1}{2}+N_z)\\ N_z\end{pmatrix}\xrightarrow[3)\ \pi J[2H_zN_z]\cdot(2J)^{-1}]{1)\ 90^{\circ}_{y}(^{1}H^{15}N)\ 2)\ 180^{\circ}_{x}(^{1}H^{15}N)}\begin{pmatrix}-H_yN_z+H_xN_x\\ \hline H_yN_z+H_xN_x\\ -2N_yH_z\end{pmatrix}\xrightarrow{90^{\circ}_{x}(^{15}N)}\begin{pmatrix}-H_yN_y+H_xN_x\\ \hline H_yN_y+H_xN_x\\ 2N_zN_z\end{pmatrix}\xrightarrow[3)\ \pi J[2H_zN_z]\cdot(2J)^{-1}]{1)\ 90^{\circ}_{y}(^{1}H)\ 2)\ 180^{\circ}_{y}(^{1}H^{15}N)}\begin{pmatrix}-H_yN_y-\frac{1}{2}N_y\\ \hline H_yN_y-\frac{1}{2}N_y\\ -H_y\end{pmatrix}\xrightarrow{90^{\circ}_{x}(^{1}H)}\begin{pmatrix}-N_y(\frac{1}{2}+H_z)\\ \hline -N_y(\frac{1}{2}-H_z)\\ -H_z\end{pmatrix}\right\}\quad(8)$$

Finally, both stored polarisation and on-resonant water magnetisation are flipped back with the echo path phase setting, ST2-PT(+), provided that water dephasing caused by gradient G_1 is compensated by an identical z-spoil gradient G_0 placed after the initial INEPT. Recording the antiecho path via ST2-PT(−), however, requires inversion of phases ϕ_5 and ϕ_{15} that would invert both stored polarisation and water by the end of scan A (cf. Equation 5b, row 3, last column). This must be prevented by simultaneously inverting phases ϕ_1, ϕ_3 and ϕ_{13}. Note that the unwanted TROSY polarisation side component is always inverted with respect to the stored anti-TROSY polarisation (cf. Equation 5b, row 6).

Modified preparatory ST2-PT module of scan B

Scan B *immediately* follows FID acquisition of the TROSY spectrum in scan A, directly exploiting the stored $H_z(\frac{1}{2}-N_z)$ anti-TROSY polarisation (term 7b). Its preparatory module must transfer magnetisation from ^{1}H to ^{15}N with an exchange of anti-TROSY to TROSY spin states, avoiding their mixing that would destroy 50% of the S^3 polarisation. With two minor modifications, this task is readily accomplished by the ST2-PT module again: (i) time-reversing and preceding the module by an initial 90° ^{1}H excitation pulse changes transfer direction from ^{1}H to ^{15}N; (ii) a 90° phase shift of the second 180°(^{1}H) pulse then swaps proton spin states once. Any remaining coherences are eliminated by the phase cycle of scan B, or an optional initial z-spoil gradient. For convenience, we set pulse phases to yield identical spectrum phases for both scans A and B. In reversion of scheme 4 we obtain the following transfers for all relevant terms present at the beginning of scan B, being the stored anti-TROSY $H_z(\frac{1}{2}-N_z)$ polarisation (row 1, term 7b), some unwanted TROSY $H_z(\frac{1}{2}+N_z)$ polarisation (row 2, term 7c), and some N_z polarisation from $T_1(N_z)$ relaxation (row 3):

The associated weighting factors ξ^{B} and ξ^{A} may differ from those valid at the end of scan A (terms 7b and 7c) due to further relaxation during the intermediate FID acquisition delay; ζ represents the fraction of N_z polarisation recovered through $T_1(N_z)$ relaxation. As described in section "Preparatory S^3-CT module of scan A", only the phase setting there determines whether natural ^{15}N polarisation enhances ($-\gamma_N$) or reduces ($+\gamma_N$) the H^N anti-TROSY polarisation exploited in scan B. Note that any recovered N_z polarisation is converted into $-H_z$ polarisation in $t_{1,B}$ and no longer contributes to the magnetisation exploited in scan B; the terminal ST2-PT module simply shuffles this polarisation back to N_z.

Terminal ST2-PT module of scan B

The terminal ST2-PT modules in scans A and B are identical and we can simply pick out the relevant terms and rows from the schemes delineated in section "Terminal ST2-PT module of scan A" in order to see how the desired TROSY coherence is transferred from ^{15}N to H^N and unambiguously separated from any unwanted anti-TROSY coherence by the triple gradient selection scheme. In contrast to scan A, however, no more immediately exploitable polarisation remains after scan B. Rather, after each pair of concatenated scans A and B, H^N polarisation needs to recover from zero during a reequilibration delay as long as in conventional TROSY experiments. This time-determining reequilibration delay is, however, omitted *within* each pair of scans A and B. Thus, ideally twice the available polarisation can be sampled by qTROSY within almost the same measurement time of a conventional TROSY experiment.

Extent of recovery and relaxation effects

The extent of anti-TROSY polarisation recovered by the qTROSY scheme is in practice compromised by several effects, with the stored magnetisation not only accumulating losses within scan B that reads it out, but also during the preceding scan A that prepares it on a distinct transfer path.

Losses from misset coupling evolution delays and pulses increase for both qTROSY scans with respect to conventional TROSY. Pulse miscalibration scales down qTROSY intensities by $\cos^{n}(\Delta_N)\cdot\cos^{N}(2\Delta_N)\cdot\cos^{h}(\Delta_H)\cdot\cos^{H}(2\Delta_H)$, where n and N (h and H) are the numbers of additional 90° and 180° pulses on ^{15}N (^{1}H), respectively, and Δ_N (Δ_H) is the error in the associated 90° pulse. Scan A differs from a conventional TROSY only by the additional S^3E module, whence n = 2, N = 1 and H = 1. Scan B correspondingly differs by one preparatory ST2-PT instead of an INEPT module, but scan A preparing the magnetisation exploited must be added, totalling n = 6 and N = h = H = 5. Assuming errors of ±2° and ±4° for the 90° ^{1}H and ^{15}N pulses, respectively, scan A would thus accumulate 1.7% and scan B 7.5% more losses than conventional TROSY. As in general, substitution with pulses that are more tolerant to miscalibration, offset effects and B_{rf} inhomogeneity might prove advantageous. Losses from incomplete antiphase evolution with respect to $^{1}J_{HN}$ add up in a similar way and can be minimised by properly setting the corresponding evolution delay Δ to $1/(2^{1}J_{HN})$. Optimising with respect to T_2 relaxation reduces this delay to $\Delta_{opt} = \arctan(\pi^{1}J_{HN}T_2)/(\pi^{1}J_{HN})$.

The effects of relaxation are more critical for qTROSY performance. Compared to conventional TROSY, scan A only suffers additional $T_2(^{15}N)$ relaxation during the short $\Delta_{opt}/2$ delay in its S^3E step. Ensuing losses (ca. 5% for an assumed $T_2(^{15}N)$ = 50 ms, with Δ_{opt} = 5.3 ms) along with pulse errors (<2%, see above) then represent the 'admission charge' to the qTROSY recovery scheme to be paid for by the appended scan B. The stored anti-TROSY magnetisation recovered here, however, invariably accumulates more substantial T_2 relaxation losses during all coupling evolution delays of both concatenated scans that it passes in diverse types of coherence (^{1}H or ^{15}N single- or multi-quantum coherence, cf. schemes 1–8). Magnetisation detected in scan B thus spends a total duration of $7.5\cdot\Delta_{opt}$ in the transverse plane, as opposed to $3.5\cdot\Delta_{opt}$ in scan A, and $3\cdot\Delta_{opt}$ in conventional TROSY; an additional $3\cdot\varepsilon$ coherence time during the three coherence-selective gradients applies in all cases. Assuming an average T_2 of 50 ms for all types of coherence, transverse relaxation losses would then reduce recovery in scan B to ca. 60% with respect to conventional TROSY, while scan A retains 95% of its intensity.

Scan B intensities are furthermore affected by T_1 relaxation during both shift evolution times $t_{1,A}$ and $t_{2,A}$ in the preceding scan A, where the recovered anti-TROSY polarisation was stored as $N_z(\frac{1}{2} - H_z)$ and $H_z(\frac{1}{2} - N_z)$ magnetisation, respectively. Of the half-depleted underlying N_z, $2N_zH_z$ and H_z components (cf. factor $\frac{1}{2}$ from spin state selection), only the latter may benefit from longitudinal relaxation driving it back to a sizeable equilibrium value, $\gamma_H\cdot H_z$. Contrarily, γ_H-hyperpolarised N_z polarisation decays to the negligibly small equilibrium value $\gamma_N\cdot N_z$, while two spin order $2N_zH_z$ vanishes altogether. Decay rates are generally dominated by the lowest possible transition frequency, for which the spectral density J(ω) is the most intense. Therefore, decay of both N_z and $2N_zH_z$ components would also proceed faster than (spin state *un*selective) recovery of $H_z = H_z(\frac{1}{2} - N_z) + H_z(\frac{1}{2} + N_z)$ polarisation, being dominated by the larger spectral density at the lower available ^{15}N transition frequency, i.e. $J(\omega_N) > J(\omega_H)$. At higher magnetic fields and with increasing molecular correlation time, all polarisations would be stabilised as J(ω) decreases. Dipolar coupling to surrounding protons, however, introduces efficient alternative relaxation pathways for the H_z component that confer a dependence on the large J(0) value (which increases with the molecular correlation time!) and may either further drain or replenish it, depending on the magnetisation of the surrounding proton lattice. A more detailed description of these complex longitudinal relaxation processes goes beyond the scope of this paper and can be found elsewhere (Wang et al., 2000; Korzhnev et al., 2001), while a semi-quantitative analysis of density matrix calculations is provided in the supplementary material. The result indicates a considerable decay for both ^{15}N and, to a lesser extent, H^N anti-TROSY polarisation during the $t_{1,A}$ and $t_{2,A}$ shift evolution times, respectively. qTROSY recoveries can

therefore be efficiently optimised by keeping these periods reasonably short, as dictated by the minimally acceptable resolution that inversely depends on the maximal evolution time, i.e. FID resolution = $(2 \cdot t_{max})^{-1}$. The simulations moreover illustrate the importance of controlling the spin temperature of the proton lattice, especially for larger proteins with efficient spin diffusion. In the end, however, the most dominant degradation factor for the recovered anti-TROSY polarisation remains T_2 relaxation during all coupling evolution delays Δ.

Experimental results and discussion

For an experimental validation, we tested the performance of the qTROSY recovery scheme on 4 different proteins: human ubiquitin (76 residues, Ubiquilable™ from VLI Research, www.vli-research.com); the ribonuclease barnase from *Bacillus amyloliquefaciens* (110 residues, BMRB 4964); the cupredoxin azurin from *Pseudomonas aeruginosa* in its reduced form (128 residues) (Karlsson et al., 1989); and the B1 domain of peptostreptococcal protein-L Y45W mutant, in the following called pL (64 residues) (Millet et al., 2003). All samples were [U−^{15}N] labeled, pL was additionally perdeuterated.

We first examined the qTROSY scheme (Figure 1) qualitatively on one-dimensional scan B spectra acquired with $t_{1,B}$ set to zero. Results are shown in Figure 2a, where the FID acquisition time $t_{2,A}$ of scan A was varied to demonstrate the effect of longitudinal relaxation on the H^N polarisation retrieved in scan B. Clearly, substantial exploitable magnetisation remains for all 4 proteins and $t_{2,A}$ times in qTROSY. As expected, this magnetisation is inherently spin state specific (Figure 2b), proving the principle of anti-TROSY polarisation storage. In contrast, conventional TROSY (without S^3E module in scan A; left column of Figure 2a) completely depletes all proton magnetisation, which then slowly recovers without spin state selectivity following the well-known saturation recovery curve. For the $H_z(\frac{1}{2} - N_z)$ anti-TROSY polarisation prepared by scan A of qTROSY, relaxation of the constituting $2H_zN_z$ component initially dominates, causing a dip in the recovery curve at a distinct $t_{2,A}$ time that correlates with the $T_1(H^N)$ relaxation time. Relaxation of the $H_z = H_z(\frac{1}{2} - N_z) + H_z(\frac{1}{2} + N_z)$ component from then on overrides, driving both stored anti-TROSY and depleted TROSY polarisations back to equilibrium, and thus degrading the initial spin state selectivity of the exploitable magnetisation. Since scan B would subsequently convert TROSY polarisation into anti-TROSY coherence, the triple gradient selection scheme here is all the more important for retaining a pure TROSY spectrum in a single scan.

Figure 2. H^N polarisation recovery in qTROSY sampled by scan B as function of the preceding inter-scan $t_{2,A}$ time. The polarisation recovery delay after scan B was set to 20 s for near-quantitative recovery; $t_{1,A} = t_{1,B} = 0$. (a) Full 1D H^N spectra acquired for the indicated proteins and NMR conditions. Columns differ in the exploitation of natural ^{15}N polarisation, as indicated. The left reference column shows H^N saturation recovery in conventional TROSY (scan A without S^3E module). While magnetisation here has to recover from zero, substantial anti-TROSY polarisation is stored and regained by the qTROSY scheme. As $t_{2,A}$ increases, this $H_z(\frac{1}{2} - N_z)$ anti-TROSY polarisation decays to a minimum (vertical line) mostly due to initial relaxation losses of the constituent $2H_zN_z$ component, which then gets compensated by spin state unselective recovery of the H_z component. Horizontal bars define initial, minimal and maximal anti-TROSY polarisation recovered. (b) Close-up on an individual, 1D resolved H^N signal of pL [U−^{15}N,^{2}H] at 600 MHz, 25 °C, illustrating the spin state selectivity of polarisation recovery in conventional TROSY and in qTROSY (recorded without use of ^{15}N polarisation). In the former, initially depleted H^N polarisation recovers without spin state selectivity. Contrarily, qTROSY preserves substantial S^3 anti-TROSY polarisation, where the initial spin state selectivity is gradually lost as the counterpart H^N TROSY polarisation recovers just as after the conventional TROSY experiment. The triple gradient selection scheme here was omitted from the pulse sequence (Figure 1) to allow observation of both TROSY and anti-TROSY components.

Figure 2a also illustrates how natural ^{15}N polarisation can be shuffled between both scans of qTROSY, effecting a positive or negative signal enhancement in scan B. This again confirms that the anti-TROSY magnetisation recovered here originates in scan A, where the shuffling of ^{15}N polarisation is exclusively controlled by phase ϕ_3 of the 90°(^{1}H) transfer pulse in the initial INEPT module; remember in this context that ^{15}N polarisation recovering during $t_{2,A}$ cannot contribute to signal intensities in scan B anymore (see section "Modified preparatory St2-PT module of scan B"). The theoretically expected enhancement by $\pm 10\%$ (i.e., $\pm \gamma_N/\gamma_H$) is, however, only achieved for zero elapse time between scans A and B (i.e.,

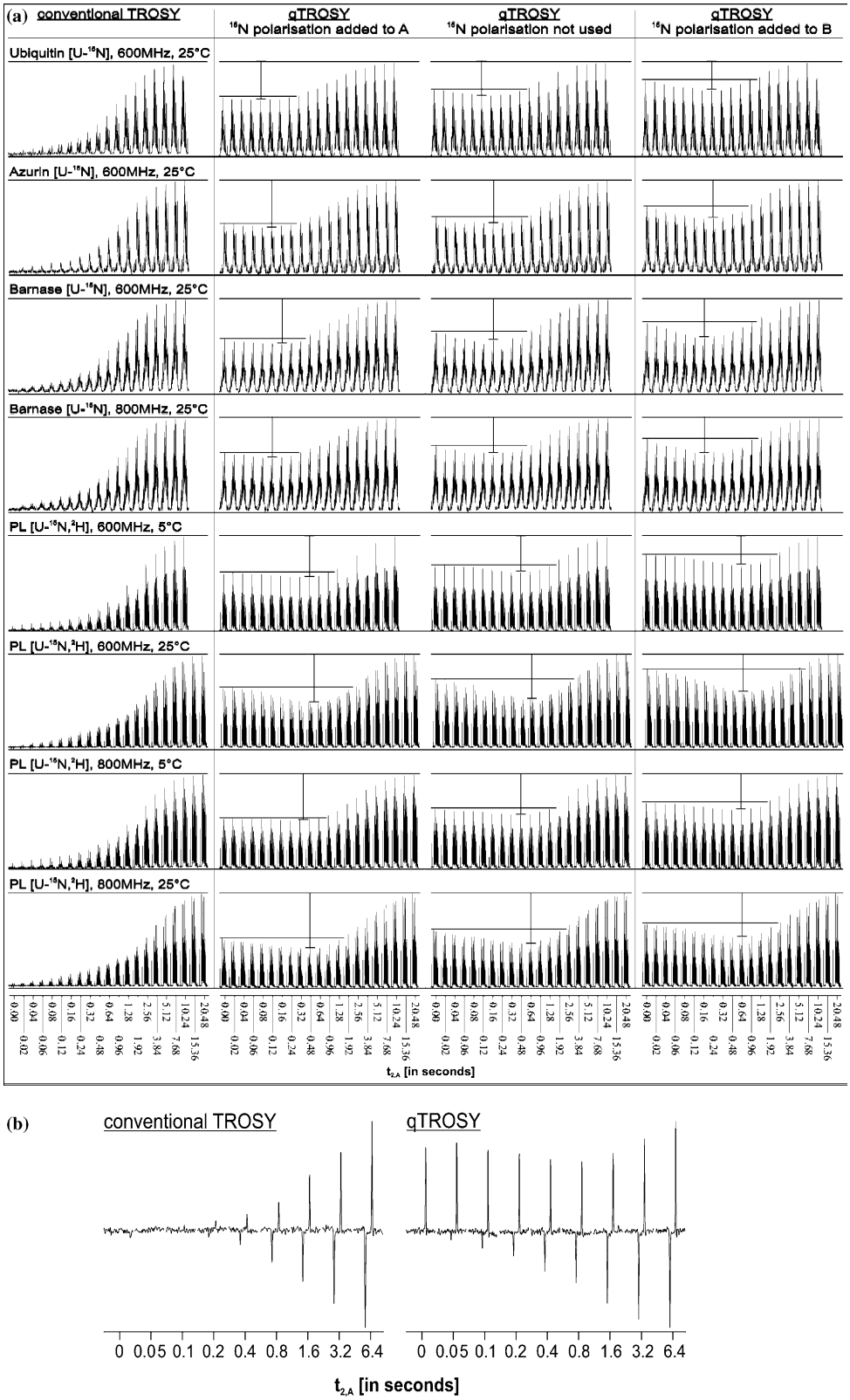
(a)
conventional TROSY
qTROSY
^{15}N polarisation added to A
qTROSY
^{15}N polarisation not used
qTROSY
^{15}N polarisation added to B
Ubiquitin [U-^{15}N], 600MHz, 25°C
Azurin [U-^{15}N], 600MHz, 25°C
Barnase [U-^{15}N], 600MHz, 25°C
Barnase [U-^{15}N], 800MHz, 25°C
PL [U-^{15}N,^{2}H], 600MHz, 5°C
PL [U-^{15}N,^{2}H], 600MHz, 25°C
PL [U-^{15}N,^{2}H], 800MHz, 5°C
PL [U-^{15}N,^{2}H], 800MHz, 25°C
0.00 0.02 0.04 0.06 0.08 0.12 0.16 0.24 0.32 0.48 0.64 0.96 1.28 1.92 2.56 3.84 5.12 7.68 10.24 15.36 20.48
$t_{2,A}$ [in seconds]

(b)
conventional TROSY
qTROSY
0 0.05 0.1 0.2 0.4 0.8 1.6 3.2 6.4
0 0.05 0.1 0.2 0.4 0.8 1.6 3.2 6.4
$t_{2,A}$ [in seconds]

$t_{2,A} = 0$). As $t_{2,A}$ increases, T_1 recovery of H^N polarisation gradually erases the prehistory of the initially stored anti-TROSY component, and with it the original ^{15}N polarisation enhancement. With little enhancement left by the $t_{2,A}$ time corresponding to minimal recovery, the depicted magnetisation recovery curves exhibit a more or less pronounced dip if ^{15}N polarisation is added to or subtracted from the anti-TROSY polarisation sampled in scan B, respectively.

In summary, Figure 2a confirms that substantial anti-TROSY $H_z(\frac{1}{2} - N_z)$ polarisation is available at all $t_{2,A}$ times. In contrast, Figure 3 illustrates how longitudinal relaxation depletes the γ_H-hyperpolarised anti-TROSY $N_z(\frac{1}{2} - H_z)$ polarisation stored during $t_{1,A}$ by driving it towards the small negative $\gamma_N \cdot N_z$ equilibrium value, where rapid proton spin flips accelerate the decay for the non-deuterated proteins. This worst-case scenario, however, only holds for $t_{2,A} = 0$ where all magnetisation recovered in scan B was prepared by the initial oS^3, and therefore fully depends on the prehistory sampled by scan A. With increasing $t_{2,A}$, this strict correlation gradually vanishes as H^N polarisation recovers independently, complementing and eventually overriding the scan A derived anti-TROSY polarisation. As a result, the decay curves sampled in Figure 3 increasingly loose their $t_{1,A}$ dependence for $t_{2,A} > 0$, flattening and levelling off at higher offsets to the benefit of the qTROSY recovery scheme. In triple resonance TROSY experiments, the incremental t_1 time is usually replaced by two constant evolution delays totalling ca. 50 ms or up to 100 ms to evolve $^1J_{NCO}$ or $^{1,2}J_{NCA}$ couplings, respectively. Relaxation losses in the ^{15}N anti-TROSY polarisation may then exceed those of its proton counterpart (Figure 2a) even if $t_{2,A}$ is set near the minimum for anti-TROSY H^N polarisation recovery. It is customary, however, to employ deuterated samples in 3D TROSY experiments in order to stabilise the ^{15}N TROSY coherence during the substantial constant time delays. Obviously, this remedy likewise benefits the stored ^{15}N anti-TROSY polarisation, as indicated by the recovery curves obtained for deuterated pL. Note that, if $t_{1,A}$ and $t_{1,B}$ are incremented synchronously, increased linewidths could result for the corresponding ^{15}N dimension in spectrum B owing to the additional T_1 relaxation modulation of the exploited anti-TROSY polarisation during $t_{1,A}$. This effect,

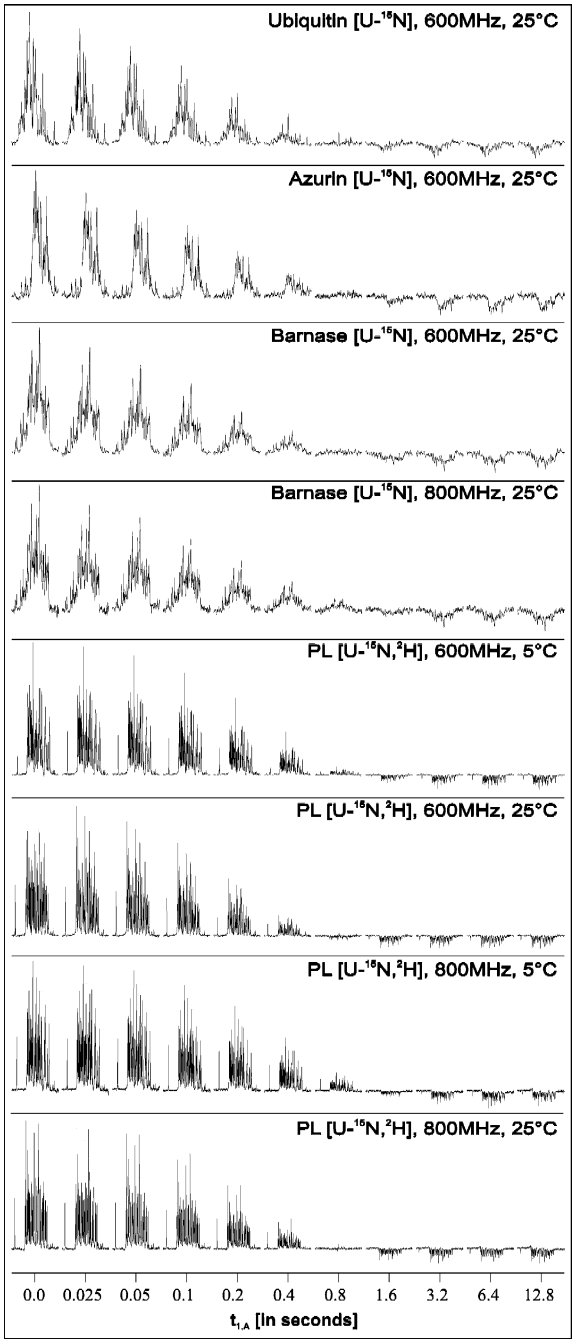

Figure 3. Polarisation recovery in qTROSY sampled by scan B as function of the preceding ^{15}N shift evolution time in scan A, $t_{1,A}$ (in ms). Shown are scan B intensities for $t_{2,A} = t_{1,B} = 0$ and the indicated proteins and NMR conditions. During this delay, the stored hyperpolarised ^{15}N anti-TROSY polarisation sampled in scan B gradually decays towards its small negative equilibrium value. As explained in the text, the decay curves flatten and level off at higher offsets with increasing $t_{2,A}$.

however, at worst doubles the ^{15}N linewidth in the unlikely case that T_1 and T_2 times become comparably short, and furthermore decreases for longer $t_{2,A}$ due to the loss in correlation between both scans (see above). In our measurements (Figure 4), the effect proved to remain well below the sampled resolution in $t_{1,B}$, and could be alleviated even by asynchronous incrementation of $t_{1,A}$ and $t_{1,B}$.

To quantify the extent of anti-TROSY polarisation recovered, we recorded two-dimensional qTROSY experiments with identical parameters

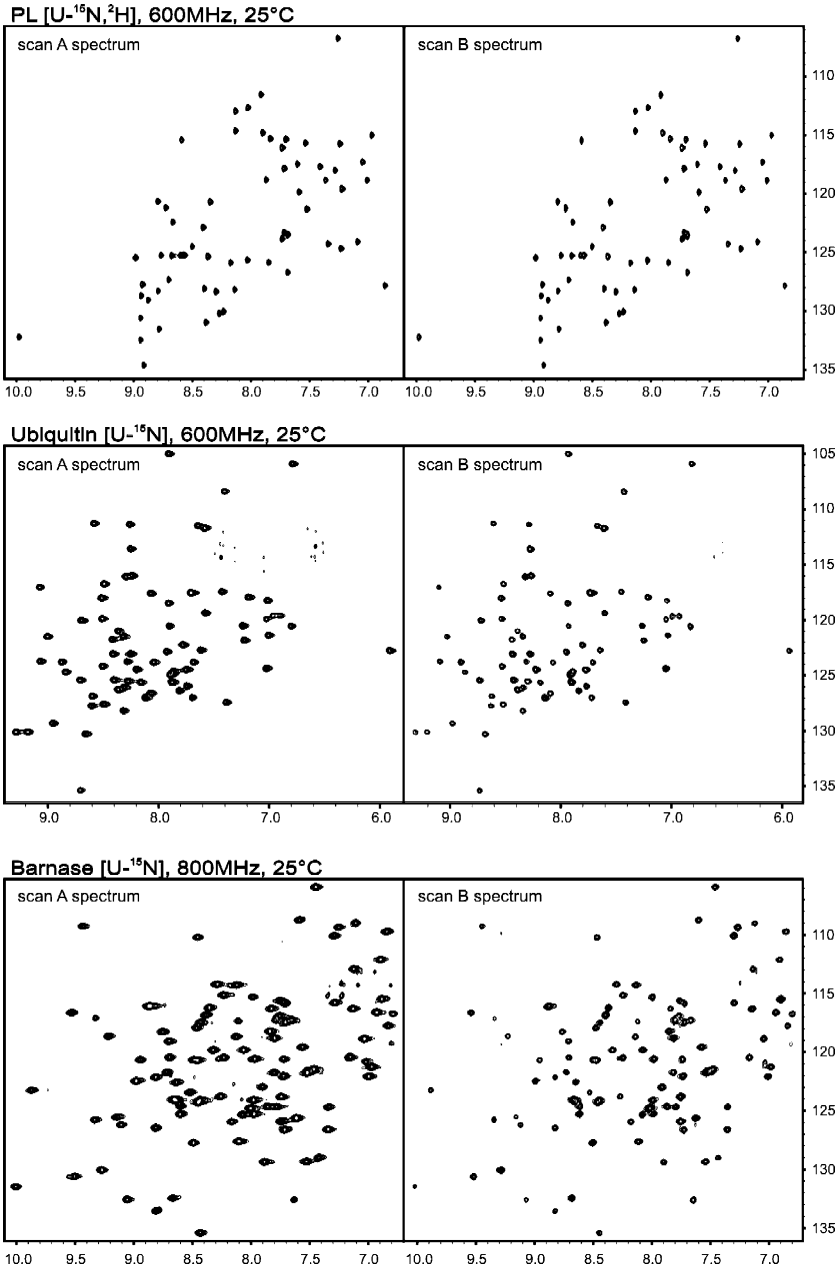

Figure 4. Representative 2D qTROSY spectrum pairs for 3 indicated test proteins and NMR conditions. Spectra were measured with the natural ^{15}N polarisation added to the anti-TROSY magnetisation exploited in scan B, and are plotted with pairwise identical contour levels. $\Delta = 5$ ms; 100 increments in t_1, resulting in a maximum $t_1 = 40$ ms; $t_{2,A}$ and $t_{2,B} = 250$ ms.

for scans A and B. As expected, both scans yielded congruent TROSY spectra (Figure 4) with no detectable difference in ^{15}N linewidths (see above). From these we determined corresponding peak intensities for all resolved signals, I_A and I_B, respectively, and calculated individual anti-TROSY polarisation recoveries as intensity ratios I_B/I_A along with mean values and standard deviations. Measurements were repeated both with and without inclusion of natural ^{15}N polarisation. We further acquired pertaining conventional TROSY spectra using only scan A of qTROSY with the S^3E module omitted and gradient G_0 inverted to preserve water flip-back, and determined corresponding peak intensities I_0. Average scan A losses were then calculated from I_A/I_0 ratios. Average overall polarisations exploited by qTROSY were derived from $(I_A+I_B)/I_0$ ratios; here, however, we always referenced against the most sensitive conventional TROSY with ^{15}N enhancement. For a conservative estimate, the FID acquisition delay t_2 was set to 250 ms throughout (corresponding to 2 Hz FID resolution), i.e. near the value for minimal proton anti-TROSY recovery (see Figure 2a). More commonly, though, acquisition delays are set to ca. 100 ms (corresponding to 5 Hz FID resolution), in which case cross-relaxation losses in the stored H^N anti-TROSY polarisation are reduced.

Histograms of qTROSY magnetisation recoveries determined for the 4 proteins at different magnetic field strengths and temperatures are shown in Figure S2 of the supplement. The data corroborates that average values and standard deviations appropriately reflect the actual distributions. Table 1 summarises all derived statistics on qTROSY performance showing that, without inclusion of natural ^{15}N polarisation, average anti-TROSY polarisation recoveries for the non-deuterated proteins range from 32% for the larger azurin (128 residues) and barnase (110 residues) to 38% for the smaller ubiquitin (76 residues) at 600 MHz and 25 °C. A substantially increased 55% average recovery was obtained for deuterated pL (64 residues), where losses in the exploited anti-TROSY magnetisation mostly from T_2 relaxation, but also some T_1 relaxation, are significantly reduced. At 800 MHz, average recoveries measured for barnase and pL decrease, again mostly due to increased T_2 relaxation losses. In contrast, lowering the temperature from 25 to 5 °C had little measurable effect for pL. When including the 10% additional natural ^{15}N polarisation, we observe good agreement with the theoretically predicted change in average recoveries (I_B/I_A) by $\pm 18\%$ that follows from the reciprocal ^{15}N polarisation enhancement on the TROSY and anti-TROSY magnetisations exploited in scans A and B, respectively (see Equations 7a and 7b; in a conventional TROSY, contrarily, all scans are uncorrelated, whence theoretical ^{15}N polarisation enhancement remains at $\pm 10\%$). By adding natural ^{15}N polarisation to the anti-TROSY polarisation, average recoveries could be boosted to well above 40% (35%) for the non-deuterated proteins and 75% (65%) for deuterated pL at 600 MHz (800 MHz).

This increase, however, comes at the price of reducing the overall magnetisation sampled by both qTROSY scans A and B mostly because T_2 relaxation degrades the additional ^{15}N polarisation more during the anti-TROSY magnetisation path exploited in scan B, for which the total coherence time is $4{\cdot}\Delta_{opt}$ longer than for the TROSY magnetisation path exploited in scan A. The latter, however, also accrues minor T_2 relaxation losses with respect to a corresponding conventional TROSY that is shorter by $0.5{\cdot}\Delta_{opt}$, lacking the S^3E module. This penalty for using the qTROSY recovery scheme in our tests amounted to ca. 5–10% losses in scan A intensities on average (Table 1), well in agreement with the previous predictions; only the elevated losses accrued for pL (but not for barnase) at 800 MHz might indicate additional errors in these measurements that suffered from deficient water flip-back. The penalty was, however, easily paid by the additional anti-TROSY magnetisation recovered in scan B, except when natural ^{15}N polarisation was piped into the latter for the larger non-deuterated proteins. Contrarily, adding this additional magnetisation to the relaxation-favoured, shorter scan A afforded maximal overall polarisation recoveries. With respect to the most sensitive ^{15}N-enhanced conventional TROSY, ca. 15–25% and up to 35% more magnetisation could thus on average be exploited for the non-deuterated proteins and deuterated pL, respectively.

While our experimental data proves that qTROSY can retrieve a sizeable amount of the anti-TROSY polarisation wasted in conventional TROSY, relaxation in practice reduces relative

Table 1. Average polarisation recovery and overall polarisation sampled with the qTROSY scheme of Figure 1, along with their standard deviations

	Ubiquitin [U–^{15}N]	Azurin [U–^{15}N]	Barnase [U–^{15}N]		pL [U–^{2}H,^{15}N]			
	600 MHz, 25 °C	600 MHz, 25 °C	600 MHz, 25 °C	800 MHz, 25 °C	600 MHz, 5 °C	800 MHz, 5 °C	600 MHz, 25 °C	800 MHz, 25 °C
Number of residues	76	128	110	110	64	64	64	64
Signals analysed	71	108	95	95	62	62	63	63
	qTROSY: Average anti-TROSY polarisation recovery = I_B/I_A (%)							
γ_N added to scan A	31.9 ± 10.2	26.1 ± 6.7	25.5 ± 5.2	22.3 ± 5.7	40.7 ± 6.5	36.5 ± 6.4	42.8 ± 4.6	35.4 ± 4.7
γ_N not used	37.9 ± 9.3	32.1 ± 6.8	32.0 ± 5.6	27.6 ± 6.4	53.3 ± 6.2	49.7 ± 6.2	55.6 ± 4.3	50.0 ± 3.9
γ_N added to scan B	46.7 ± 8.2	41.3 ± 7.9	41.5 ± 7.4	34.4 ± 7.4	71.9 ± 7.3	64.4 ± 7.1	75.2 ± 5.2	64.4 ± 3.8
	qTROSY: Average overall polarisation recovery = $(I_A + I_B)/I_0$ (%)							
γ_N added to scan A	125.3 ± 9.1	118.3 ± 7.7	117.8 ± 5.8	112.9 ± 5.4	133.5 ± 7.0	122.3 ± 6.3	136.9 ± 4.6	120.7 ± 5.0
γ_N not used	115.9 ± 10.7	106.3 ± 9.3	104.8 ± 6.5	101.6 ± 6.0	126.0 ± 8.8	116.2 ± 7.7	130.0 ± 5.7	115.5 ± 5.9
γ_N added to scan B	107.1 ± 13.7	94.3 ± 9.8	92.3 ± 7.4	89.6 ± 6.3	117.6 ± 9.2	103.0 ± 8.3	122.0 ± 7.2	100.3 ± 6.4
	qTROSY: Average scan A losses = $1-(I_A/I_0')$ (%)							
Independent of γ_N	5.2 ± 1.9	6.3 ± 3.1	6.4 ± 2.6	7.9 ± 1.6	5.4 ± 1.6	11.2 ± 1.6	4.3 ± 1.2	11.2 ± 2.1

Statistics were determined using the indicated number of signals for the denoted 4 proteins at different NMR conditions, with the natural ^{15}N polarisation γ_N included as specified. Anti-TROSY polarisation recoveries were calculated from intensity ratios I_B/I_A for corresponding signals in the 2D TROSY spectra of scans B and A. Overall polarisation recoveries were obtained from sums of scan A and B intensities, divided by the corresponding intensity I_0 in a conventional ^{15}N polarisation enhanced TROSY. The latter was measured using only scan A of qTROSY with the S^{3}E module omitted, gradient G_0 inverted and ^{15}N polarisation added to scan A, within the same total experiment time. Average intensity losses in scan A are referenced against corresponding intensities I_0' in a conventional TROSY with the same use of ^{15}N polarisation, and therefore remain independent of γ_N (note that $I_0' = I_0$ only holds for ^{15}N polarisation enhancement shuffled to scan A!). $\Delta = 5$ ms, $t_{2,A} = 250$ ms, i.e. near the value for minimal recovery (see Figure 2a).

overall polarisation recoveries to far below the theoretical maximum of 200%. qTROSY therefore performs best with small and deuterated proteins. Yet even for these, it seems hardly possible to enhance sensitivities with respect to an optimised conventional TROSY experiment through spectral addition of scans A and B: as this involves a concomitant noise accumulation by $\sqrt{2}$, relative overall polarisation recoveries would still have to exceed 140%.

We therefore propose qTROSY as a partitioning, rather than a sensitivity enhancing, scheme to split the initial H^N magnetisation into two quanta, the ratio of which can be tuned via inclusion of natural ^{15}N polarisation. Two *different* (multidimensional) TROSY-type experiments may then be concatenated into a single *asymmetric* qTROSY experiment, almost halving the overall measurement time by eliminating every other time limiting reequilibration delay. qTROSY should therefore be employed preferably in cases where experiment times are limited by the required resolution, rather than sensitivity; the implemented triple gradient selection scheme thereby ensures S^3 coherence selection in a single scan. This resolution-limited regime is particularly pronounced for deuterated proteins with their long $T_1(H^N)$ times of several seconds. Such substrates are at the same time best suited for the qTROSY scheme because of likewise reduced T_2 relaxation during all $^1J_{HN}$ evolution delays – the single most limiting factor for anti-TROSY polarisation recovery; secondary T_1 relaxation losses can generally be minimised by keeping chemical shift evolution times as small as required for meaningful FID resolutions. Favourably long T_2 times are also found particularly for smaller non-deuterated proteins. Here, HSQC-type experiments are customarily favoured since relaxation and resolution gains always afforded by TROSY spin state selection do not yet pay its price of discarding the 50% anti-TROSY polarisation part. While our data suggests that a sensitivity enhancement would likely be impossible, qTROSY could still recover enough anti-TROSY polarisation for a complete scan B experiment. Running qTROSY asymmetrically, with two different ($n > 2$ dimensional) TROSY-type experiments compacted into one, would then afford up to 50% time saving and thus make spin state selection economical nevertheless. A direct comparison of the inseparable HSQC experiment and the asymmetric qTROSY partitioning scheme is therefore neither valid nor meaningful. Only completeness of the scan B spectrum (i.e., sufficient signal-to-noise ratio) determines whether the qTROSY scheme is useful and applicable in a given case. Obviously, the more sensitive of both concatenated TROSY experiments should always be measured in the more relaxation-degraded scan B, where some adjustment of the magnetisation distribution between both qTROSY scans is possible through inclusion of the natural ^{15}N polarisation. For example, one may envisage an asymmetric 3D HNCA/HN[CO]CA-qTROSY in which scan A samples an HNCA-TROSY while scan B records the more sensitive complementary HN[CO]CA-TROSY (to be published soon).

Conclusion

We have introduced queued TROSY (qTROSY) as a novel scheme to partially recover anti-TROSY polarisation in two concatenated scans A and B. Due mostly to transverse relaxation losses, however, polarisation recovery appears insufficient for sensitivity enhancement (by adding both scans) with respect to the most sensitive, ^{15}N polarisation enhanced conventional TROSY. We therefore propose to exploit the anti-TROSY polarisation recovered in scan B for a separate experiment. We are currently investigating this application of asymmetric qTROSY as a partitioning scheme for the H^N polarisation to simultaneously feed two different, concatenated (multi-dimensional) TROSY-type experiments. Omitting every other interscan reequilibration delay can reduce overall measurement time by up to 50% for substrates with long T_1 relaxation times, sensitivity permitting. Deuterated and small non-deuterated proteins afford the largest anti-TROSY polarisation recoveries due to minimal T_2 relaxation losses. The compacting of measurement times would thus extend the attractiveness and rentability of TROSY-type spectroscopy to smaller molecular weights.

Supplementary material

Supplementary material is available (at http://dx.doi.org/10.1007/s10858-005-5618-z) containing

the results of density matrix simulations to assess the effect of T_1 relaxation on the stored anti-TROSY polarisations, as well as histograms of experimentally obtained recoveries.

Acknowledgements

This work was supported by Grant 621-2001-3095 from the Swedish Research Council. Experiments were performed at the Swedish NMR Center using proteins kindly provided by Göran Karlsson (azurin), Lewis.E. Kay (protein L) and Alexander S. Arseniev (barnase).

References

Andersson, A., Annila, A. and Otting, G. (1998) *J. Magn. Reson.* **133**, 364–367.

Czisch, M. and Boelens, R. (1998) *J. Magn. Reson.* **134**, 158–160.

Karlsson, B.G., Pascher, T., Nordling, M., Arvidsson, R.H.A. and Lundberg, L.G. (1989) *FEBS Lett.* **246**, 211–217.

Korzhnev, D.M., Billeter, M., Arseniev, A.S. and Orekhov, V.Y. (2001) *Progr. NMR Spectr.* **38**, 197–266.

Meissner, A., Duus, J.O. and Sorensen, O.W. (1997) *J. Biomol. NMR* **10**, 89–94.

Meissner, A., Schulte-Herbrüggen, T., Briand, J. and Sorensen, O.W. (1998a) *Mol. Phys.* **95**, 1137–1142.

Meissner, A., Schulte-Herbrüggen, T. and Soerensen, O.W. (1998b) *J. Am. Chem. Soc.* **120**, 7989–7990.

Millet, O., Mittermaier, A., Baker, D. and Kay, L.E. (2003) *J. Mol. Biol.* **329**, 551–563.

Palmer, A.G., Cavanagh, J., Wright, P.E. and Rance, M. (1991) *J. Magn. Reson.* **93**, 151–170.

Pervushin, K.V., Riek, R., Wider, G. and Wüthrich, K. (1997) *Proc. Natl. Acad. Sci. USA* **94**, 12366–12371.

Pervushin, K.V., Wider, G. and Wüthrich, K. (1998) *J. Biomol. NMR* **12**, 345–348.

Schulte-Herbrüggen, T., Briand, J., Meissner, A. and Soerensen, O.W. (1999) *J. Magn. Reson.* **139**, 443–446.

Sklenar, V. (1995) *J. Magn. Reson. A* **114**, 132–135.

Soerensen, O.W., Eich, G.W., Levitt, M.H., Bodenhausen, G. and Ernst, R.R. (1983) *Progr. NMR Spectr.* **16**, 163–192.

Wang, L., Kurochkin, A.V. and Zuiderweg, E.R.P. (2000) *J. Magn. Reson.* **144**, 175–185.

Weigelt, J. (1998) *J. Am. Chem. Soc.* **120**, 10778–10779.